

Matrix elements relevant for $I = 1=2$ rule and " $0=$ " from Lattice QCD with staggered fermions

D . Pekurovsky and G . Kilcup

Department of Physics,
the Ohio State University,
174 W . 18th Ave., Columbus OH 43210, USA

Abstract

We perform a study of matrix elements relevant for the $I = 1=2$ rule and the direct CP-violation parameter " $0=$ " from first principles by computer simulation in Lattice QCD. We use staggered (Kogut-Susskind) fermions, and employ the chiral perturbation theory method for studying $K^0 \bar{K}^0$ decays. Having obtained a reasonable statistical accuracy, we observe an enhancement of the $I = 1=2$ amplitude, consistent with experiment within our large systematic errors. Finite volume and quenching effects have been studied and were found small compared to noise. The estimates of " $0=$ " are hindered by large uncertainties associated with operator matching. In this paper we explain the simulation method, present the results and address the systematic uncertainties.

1 Introduction

In those areas of particle phenomenology which require addressing non-perturbative effects, Lattice QCD plays an increasingly significant role, being a first-principles method. The rapid advances in computational performance as well as algorithmic techniques are allowing for better control of various errors associated with lattice calculations.

In this paper we address the phenomenology of $K^0 \rightarrow \pi^+ \pi^-$ decays. One of the long-standing puzzles is the “ $I = 1=2$ rule”, which is the observation that the transition channel with isospin changing by $1/2$ is enhanced 22 times with respect to the one with isospin changing by $3/2$. The strong interactions are essential for explaining this effect within the Standard Model. Since the energy scales involved in these decays are rather small, computations in quantum chromodynamics (QCD) have to be done using a non-perturbative method such as Lattice QCD. In particular, Lattice QCD is used to calculate hadronic matrix elements of the operators appearing in the effective weak Hamiltonian.

There have been so far several other attempts to study matrix elements of the operators relevant for $I = 1=2$ rule on the lattice [3, 4, 6], but they fell short of desired accuracy. In addition, several groups [7, 5] have studied matrix elements $h^+ \bar{p}_i K^+ i$, which describe only $I = 3=2$, not $I = 1=2$ transition. In the present simulation, the statistics is finally under control for $I = 1=2$ amplitude.

Our main work is in calculating matrix elements $h^+ \bar{p}_i K^+ i$ and $h \bar{p}_i K^0 i$ for all basis operators (introduced in Sec. 2.1). This is enough to recover matrix elements $h^- \bar{p}_i K^0 i$ using chiral perturbation theory in the lowest order, although this procedure suffers from uncertainties arising from ignoring higher orders (in particular, final state interactions). The latter matrix elements are an essential part of the phenomenological expressions for $I = 1=2$ and $I = 3=2$ amplitudes, as well as “ $0=$ ”. The ratio of the amplitudes computed in this way contains significant enhancement of $I = 1=2$ channel, although systematic uncertainties preclude a definite answer.

In addition, we address a related issue of “ $0=$ ” { the direct CP-violation parameter in the neutral kaon system. As of the day of writing, the experimental data are somewhat ambiguous about this parameter: the group at CERN (NA48) [1] reports $\text{Re}(\text{“}0\text{=“}) = (23 \pm 7) \cdot 10^{-4}$; while the Fermilab group (E731) [2] has found $\text{Re}(\text{“}0\text{=“}) = (7.4 \pm 6.0) \cdot 10^{-4}$. There is a hope that the discrepancy between the two reports will soon be removed in a new generation of experiments.

On the theoretical side, the progress in estimating “ $0=$ ” in the Standard Model is largely slowed down by the unknown matrix elements [11] of the appropriate operators. The previous attempts [3, 4, 6] to compute them on the lattice did not take into account operator matching. In this work we repeat this calculation with better statistics and better investigation of

systematic uncertainties. We are using perturbative operator matching. In some cases it does not work, so we explore alternatives and come up with a partially non-perturbative renormalization procedure. The associated errors are estimated to be large. This is currently the biggest stumbling block in computing " η^0 ".

The paper is structured as follows. In the Section 2 we show the context of our calculations, define the quantities we are looking after and discuss a number of theoretical points relevant for the calculation. Section 3 discusses issues pertaining to the lattice simulation. In Section 4 we present the results and discuss systematic errors for $I = 1=2$ rule amplitudes. In Section 5 we explain how the operator matching problem and other systematic errors prevent a reliable calculation of " η^0 ", and give our best estimates for this quantity in Section 6. Section 7 contains the conclusion. In Appendices we give details about the quark operators and sources, and provide explicit expressions for all contractions and matrix elements for reference purposes.

2 Theoretical framework

2.1 Framework and definitions

The standard approach to describe the problems in question is to use the Operator Product Expansion at the M_W scale and use the Renormalization Group equations to translate the effective weak theory to more convenient scales ($\sim 2\{4$ GeV). At these scales the effective Hamiltonian for $K^+ \rightarrow \eta^0 \pi^+$ decays is the following linear superposition [11]:

$$H_W^e = \frac{G_F}{2} V_{ud} V_{us} \sum_{i=1}^{X^0 h} z_i(\mu) + y_i(\mu) O_i(\mu); \quad (1)$$

where z_i and y_i are Wilson coefficients (currently known at two-loop order), $V_{td} V_{ts} = V_{ud} V_{us}$, and O_i are basis of four-fermion operators defined as follows:

$$O_1 = (s \quad (1 \quad 5)u) (u \quad (1 \quad 5)d) \quad (2)$$

$$O_2 = (s \quad (1 \quad 5)u) (u \quad \overset{X}{X} \quad (1 \quad 5)d) \quad (3)$$

$$O_3 = (s \quad (1 \quad 5)d) (q \quad (1 \quad 5)q) \quad (4)$$

$$O_4 = (s \quad (1 \quad 5)d) \overset{X^q}{(q \quad (1 \quad 5)q)} \quad (5)$$

$$O_5 = (s \quad (1 \quad 5)d) \overset{X^q}{(q \quad (1 + 5)q)} \quad (6)$$

$$O_6 = (s \quad (1 \quad 5)d \quad) \underset{q}{\overset{X}{\rightarrow}} (q \quad (1 + 5)q \quad) \quad (7)$$

$$O_7 = \frac{3}{2} (s \quad (1 \quad 5)d \quad) \underset{q}{\overset{X}{\rightarrow}} e_q (q \quad (1 + 5)q \quad) \quad (8)$$

$$O_8 = \frac{3}{2} (s \quad (1 \quad 5)d \quad) \underset{q}{\overset{X}{\rightarrow}} e_q (q \quad (1 + 5)q \quad) \quad (9)$$

$$O_9 = \frac{3}{2} (s \quad (1 \quad 5)d \quad) \underset{q}{\overset{X}{\rightarrow}} e_q (q \quad (1 \quad 5)q \quad) \quad (10)$$

$$O_{10} = \frac{3}{2} (s \quad (1 \quad 5)d \quad) \underset{q}{\overset{X}{\rightarrow}} e_q (q \quad (1 \quad 5)q \quad) \quad (11)$$

Here and are color indices, e_q is quark electric charge, and summation is done over all light quarks.

Isospin amplitudes are defined as

$$A_{0,2} e^{i\phi_{0,2}} \quad h(\quad)_{I=0,2} \mathcal{H}_W \mathcal{K}^0 i; \quad (12)$$

where $\phi_{0,2}$ are the final state interaction phases of the two channels. The $I = 1=2$ rule is expressed as follows:

$$! = \text{Re}A_0 = \text{Re}A_2 = 22.2; \quad (13)$$

Direct CP violation parameter W^0 is defined in terms of imaginary parts of these amplitudes:

$$W^0 = \frac{\text{Im} A_0 - \text{Im} A_2}{2! \text{Re} A_0} e^{i(-2\phi_2 - \phi_0)}; \quad (14)$$

Experiments are measuring the ratio $W^0 =$, which is given by

$$\frac{W^0}{W} = \frac{G_F}{2! \mathcal{H} \mathcal{R} \text{Re} A_0} \text{Im} \quad t \quad [\phi_0 - \phi_2]; \quad (15)$$

where

$$t_0 = \underset{i}{\overset{X}{\sum}} y_i h(\quad)_{I=0} \mathcal{D}_i \mathcal{K}^0 i (1 + \phi_0) \quad (16)$$

$$t_2 = \underset{i}{\overset{X^1}{\sum}} y_i h(\quad)_{I=2} \mathcal{D}_i \mathcal{K}^0 i \quad (17)$$

with $\text{Im} \quad t = \text{Im} V_{td} V_{ts}$, and where $\phi_0 = 0.25 \quad 0.05$ takes into account the effect of isospin breaking in quark masses ($m_u \neq m_d$).

2.2 Treatment of charm quark

The effective Hamiltonian given above is obtained in the continuum theory in which the top, bottom and charm quarks are integrated out. (In particular, the summation in Eqs. (4{11) is done over u, d and s quarks.) This implies that the scale Λ is not much higher than the charm quark mass. Otherwise the charm quark cannot be integrated out and the effective Hamiltonian should include an additional set of operators. The lattice treatment of charm quark is in principle possible but in practice quite limited, for example by having to work at much smaller lattice spacings and having an even more complicated set of operators and contractions than the one without charm. Therefore we have opted to work in the effective theory in which the charm quark is integrated out. This is possible even if the scale Λ is slightly above the charm quark mass (typically, we take $\Lambda = 2.0 \text{ GeV}$).

2.3 Calculating $h^+ \mathcal{D}_i \bar{K}^0 i$.

As was shown by Martinelli and Testa [13], two-particle hadronic states are very difficult to construct on the lattice (and in general, in any Euclidean description). We have to use an alternative procedure to calculate the matrix elements appearing in Eqs. (12,16,17). We choose the method [10] in which lowest-order chiral perturbation theory is used to relate $h^+ \mathcal{D}_i \bar{K}^0 i$ to matrix elements involving one-particle states:

$$h^+ \mathcal{D}_i \bar{K}^0 i = \frac{m_K^2 - m^2}{f} \quad (18)$$

$$h^+ \mathcal{D}_i \bar{K}^+ i = (\bar{p} \bar{p}) \frac{m_s + m_d}{f} \quad (19)$$

$$h^0 \mathcal{D}_i \bar{K}^0 i = (m_s - m_d); \quad (20)$$

where f is the lowest-order pseudoscalar decay constant. Masses in the first of these formulae are physical meson masses, while masses of quarks and momenta in the other two formulae are meant to be from actual simulations on the lattice (the latter are done with unphysical masses). These relationships ignore higher order terms in the chiral expansion, most importantly the final state interactions. Thus any results obtained with this method suffer from a significant uncertainty. The the sign of the higher-order corrections is likely to be different for $I = 1=2$ and $I = 3=2$ amplitudes: positive for the former (due to final state interactions) and negative for the latter (see Golterman and Leung [16]).

3 Lattice techniques

3.1 Mixing with lower-dimensional operators.

Eqs. (18{20) implicitly handle unphysicals \$ d mixing in $h^+ \bar{p}_i \bar{K}^+ i$ by subtracting the unphysical part proportional to $h^0 \bar{p}_i \bar{K}^0 i$. This is equivalent to subtracting the operator

$$O_{\text{sub}} = (m_d + m_s)s d + (m_d - m_s)s_5 d; \quad (21)$$

As shown in Refs. [8, 9], these statements are also true on the lattice if one uses staggered fermions. A number of Ward identities discussed in these references show that lattice formulation with staggered fermions retains the essential chiral properties of the continuum theory. In particular, only one lower-dimensional operator appears in mixing with the basis operators. (Lower-dimensional operators have to be subtracted non-perturbatively since they are multiplied by powers of a^{-1} .) We employ the non-perturbative procedure suggested in Ref. [9]:

$$h^+ \bar{p}_i \bar{K}^0 i = h^+ \bar{p}_i - i O_{\text{sub}} \bar{K}^+ i \frac{m_K^2 - m^2}{(p - p_f)^2}; \quad (22)$$

where i are found from

$$0 = h^0 \bar{p}_i - i O_{\text{sub}} \bar{K}^0 i; \quad (23)$$

which allows subtraction $time slice$ by $time slice$. This procedure is equivalent to the lattice version of Eqs. (18{20).

Throughout our simulation we use only degenerate mesons, i.e. $m_s = m_d = m_u$. Since only negative parity part of O_{sub} contributes in Eq. (23), one naively expects 0 in Eq. (23) when calculating i . However, we notice that matrix elements $h^0 \bar{p}_i \bar{K}^0 i$ vanish for all basis operators if $m_s = m_d$. This is due to invariance of both the Lagrangian and all the operators in question under the CPS symmetry, which is defined as CP symmetry combined with interchange of s and d quarks. Thus the calculation of i requires taking the first derivative of $h^0 \bar{p}_i \bar{K}^0 i$ with respect to $(m_d - m_s)$. In order to evaluate the first derivative numerically, we insert another fermion matrix inversion in turn into all propagators involving the strange quark. The detailed expressions for all contractions are given in the Appendices.

3.2 Diagrams to be computed

According to Eqs. (22,23), we need to compute three diagrams involving four-fermion operators (shown in Fig. 1) and a couple of bilinear contractions. The "ghost" contraction type (Fig. 1a) is relatively cheap to compute. The "eye" and "annihilation" diagrams (Fig. 1b)

and 1c) are much more expensive since they involve propagator loops for every point in space-time.

3.3 Lattice parameters and other details

The parameters of simulation are listed in the Table 1. We use periodic boundary conditions in both space and time. Our main "reference" ensemble is a set of quenched configurations at $6=g^2 = 6.0$ (Q_1). In addition, we use an ensemble with a larger lattice volume (Q_2), an ensemble with $6=g^2 = 6.2$ (Q_3) for checking the lattice spacing dependence, and an ensemble with 2 dynamical flavors ($m = 0.01$) generated by the Columbia group, used for checking the impact of quenching. The ensembles were obtained using 4 sweeps of SU(2) overrelaxed and 1 sweep of SU(2) heatbath. The configurations were separated by 1000 sweeps, where one sweep includes three SU(2) subgroups updates. We use the standard staggered fermions action. Conjugate gradient is used for fermion propagator calculations. Jackknife is used for statistical analysis.

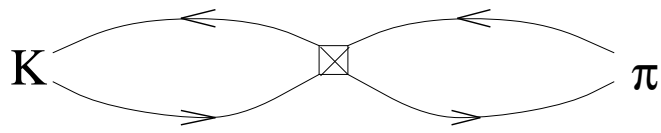
Table 1: Simulation parameters

Ensemble name	N_f	Size		$L, \text{ fm}$	Number of configurations	Quark masses used	
Q_1	0	6.0	16^3	(32 4)	1.6	216	0.01 0.05
Q_2	0	6.0	32^3	(64 2)	3.2	26	0.01 0.05
Q_3	0	6.2	24^3	(48 4)	1.7	26	0.005 0.03
D	2	5.7	16^3	(32 4)	1.6	83	0.01 0.05

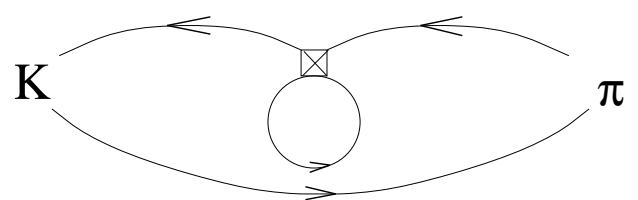
As explained below, we have extended the lattice 4 times for all ensembles (except 2 times for the biggest volume) in time dimension by copying gauge links. This is done in order to get rid of excited states contamination and wrap-around effects.

The lattice spacing values for quenched ensembles were obtained by performing a fit in the form of the asymptotic scaling to the quenched data of meson mass given elsewhere [15]. Lattice spacing for the dynamical ensemble is also set by the mass [14].

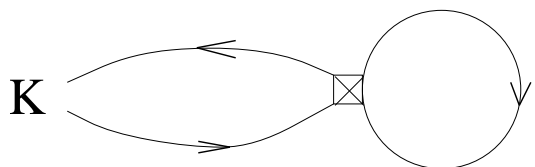
Some other technicalities are as follows. We work in the two flavor formalism. We use local wall sources that create pseudoscalar mesons at rest. (Smearing did not have a substantial effect.) We use staggered fermions and work with gauge-invariant operators, since the gauge symmetry enables significant reduction of the list of possible mixing operators. The staggered flavor structure is assigned depending on the contraction type. Our operators are tadpole-improved. This serves to "improve" the perturbative expansion at a later stage when



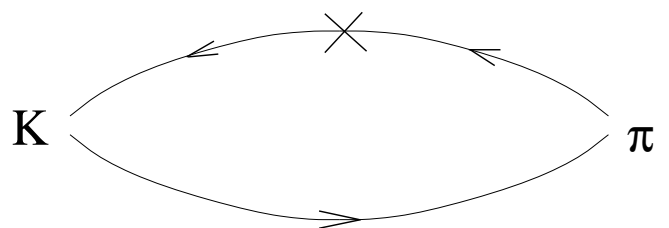
(a)



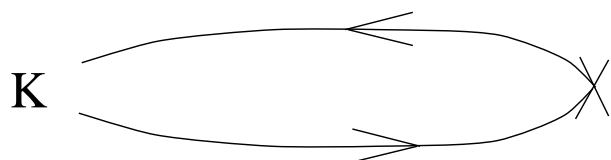
(b)



(c)



(d)



(e)

Figure 1: Five diagrams types needed to be computed: (a) \Eight"; (b) \Eye"; (c) \Annihilation"; (d) \Subtraction"; (e) two-point function.

we match the lattice and continuum operators. For calculating fermion loops we employ the U(1) pseudofermion stochastic estimator. More details and explanation of some of these terms can be found in the Appendices.

3.4 Setup for calculating matrix elements of four-fermion operators

For simplicity, consider the setup for the calculation of "eight" contractions. Kaons are created at time $t = 0$, the operators are inserted at a variable time t , and the pion sink is at a much later time T (see Fig. 2). In principle, a number of states with the same quantum numbers can be created by the source. Each state's contribution is proportional to $Z e^{m t_j}$, so the lightest state (kaon) dominates at large enough t . Analogously, states annihilated by the sink contribute proportionally to $Z e^{m \bar{T} t_j}$, which is dominated by the pion.

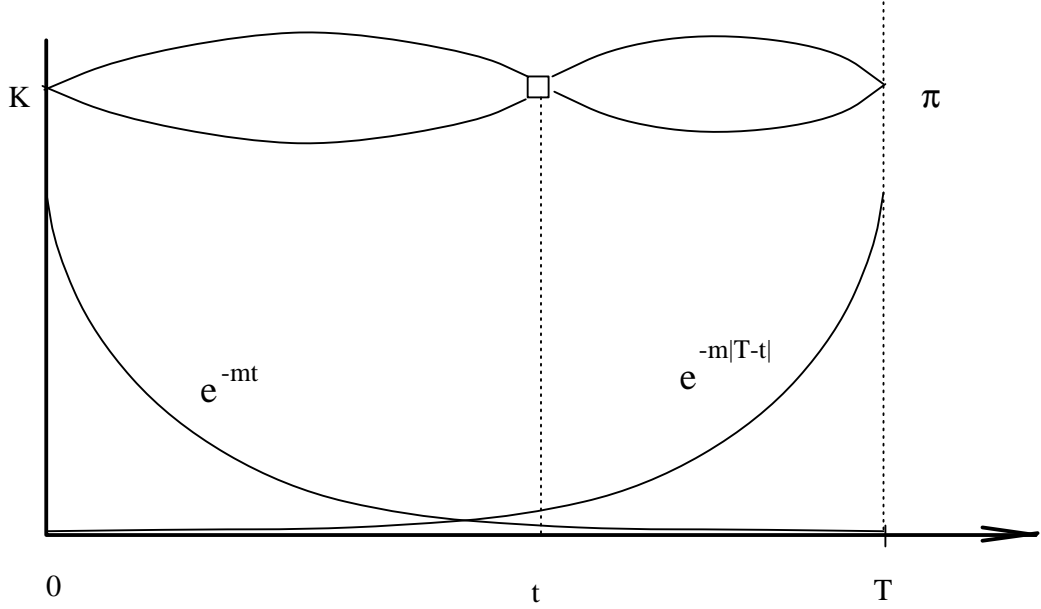


Figure 2: The general setup of the simulation. An "eight" contraction is shown for convenience. The kaon source is at the time slice 0, while the pion sink is at the time slice T . The operator is inserted at a variable time t . The result of this contraction is proportional to the product of two exponentials shown in the figure.

In this work kaon and pion have the same mass and therefore are technically the same. In the middle of the lattice, where t is far enough from both 0 and T , we expect to see a plateau, corresponding to $Z e^m T h \bar{J} K i$. This plateau is our working region.

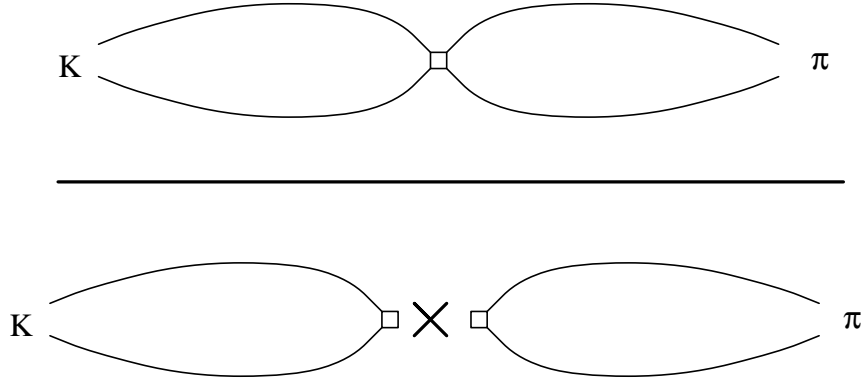


Figure 3: B ratio is formed by dividing the four-fermion matrix element by the product of two-point functions, typically involving A or P bilinears. All the operators involved are inserted at the same time slice t , and the external meson sources are also located at the same time slices. This enables cancellation of various common factors.

3.5 B ratios

It is sometimes convenient to express the results for matrix elements in terms of so-called B ratios, which are the ratios of desired four-fermion matrix elements to their values obtained by vacuum saturation approximation (VSA). For example, the B ratios of operators O_2 and O_4 is formed by dividing the full matrix element of a given operator by the product of two-point functions (Fig. 3). We expect the denominator of the ratio to form a plateau in the middle of the lattice, equal to $Z e^m T h \bar{J} K i = h \bar{J} K i$, where A are the axial vector currents with appropriate flavor quantum numbers for kaon and pion. Thus, in the B ratio the factor $Z e^m T$ cancels, leaving the desirable ratio $h \bar{J} K i = (h \bar{J} K i - h \bar{J} K i)$. Apart from common normalization factors, a number of systematic uncertainties also tend to cancel in this ratio, including the uncertainty in the lattice spacing, quenching and in some cases perturbative correction uncertainty. Therefore, it is sometimes reasonable to give lattice answers in terms of the B ratios.

However, eventually the physical matrix element needs to be reconstructed by using the known experimental parameters (such as f_K) to compute VSA. In other cases, such as for operators O_5 | O_8 , the VSA itself is known very imprecisely due to the failure of perturbative matching (see Sec. 5). Then it is more reasonable to give answers in terms of matrix elements in physical units. We have adopted the strategy of expressing all matrix elements in units of $\langle \bar{K} \rangle \langle K \rangle = (f_K^{\text{latt}})^2 m_K^2$ at an intermediate stage, and using pre-computed f_K^{latt} at the given meson mass to convert to physical units. This method is sensitive to the choice of the lattice spacing.

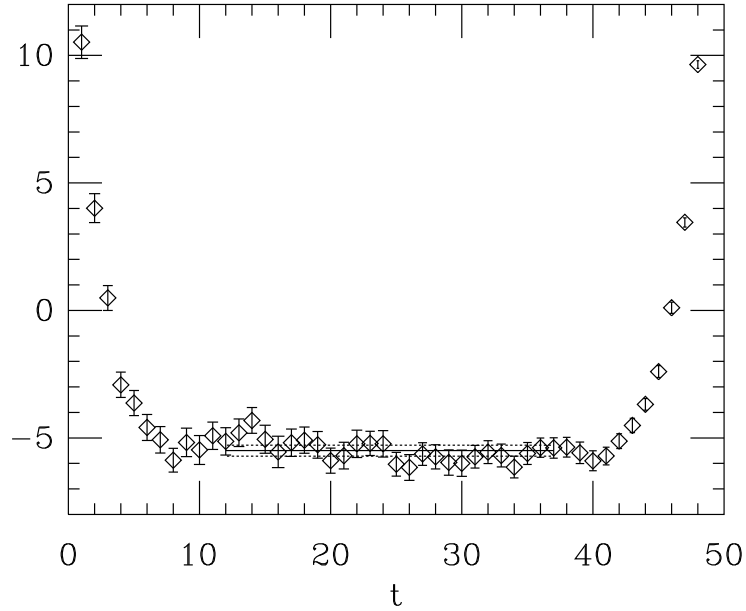


Figure 4: An example of the signal we get for one of the B ratios (in this case, for the "eye" part of the O_2 operator on Q_1 ensemble). The wall sources are at $t = 1$ and $t = 49$. We see that the excited states quickly disappear and a stable, well-distinguished plateau is observed. We perform jackknife averaging in the range of t from 12 to 37 (shown with the horizontal lines). It is important to confirm the existence of the plateau for reliability of the results.

It is very important to check that the time distance between the kaon and pion sources T is large enough so that the excited states do not contribute. That is, the plateau in the middle of the lattice should be sufficiently flat, and the B ratios should not depend on T . We have found that in order to satisfy this requirement the lattice has to be artificially extended

in time direction by using a number of copies of the gauge fields (4 in the case of the small volume lattices, 2 otherwise). We are using $T = 72$ for Q_3 ($\kappa = 0.2$) ensemble, and $T = 48$ for the rest. An example of a plateau that we obtain with this choice of T is shown in Fig. 4. To read off the result, we average over the whole extension of the plateau, and use jackknife to estimate the statistical error in this average.

4 $I = 1=2$ rule results

Using the data obtained from matrix elements of basis operators, in this section we show the numerical results for $I = 1=2$ and $I = 3=2$ amplitudes as well as their ratio.

4.1 $\text{Re}A_2$ results

The expression for $\text{Re}A_2$ can be written as

$$\text{Re}A_2 = \frac{G_F}{P} V_{ud} V_{us} z_+ (\lambda) h_{O_+} i_2;$$

where

$$h_{O_+} i_2 = h(\lambda) \bar{O}_2 \not{p}_1 + O_2 \not{K} i = \frac{4}{9} \frac{P}{2} f_K (m_K^2 - m^2) B_+(\lambda);$$

Here $z_+(\lambda)$ is a Wilson coefficient and $B_+(\lambda)$ is the B ratio of the O_+ operator. In the lowest-order chiral perturbation theory, and in the limit of preserved $SU(3)$ flavor symmetry, it can be shown that

$$B_+ = B_K;$$

where B_K is the B ratio for the neutral kaon mixing operator $O_K = \bar{s}_L d \bar{s}_L d$, given by $\bar{h} \not{K}^0 \not{p}_K \not{K}^0 i = \frac{8}{3} m_K^2 f_K^2 B_K$. This matrix element involves only "eight" diagrams. It has been studied by a number of groups [18, 19], and is currently known quite reliably within the quenched approximation. The chiral behaviour is expected to have the form $B_K = a + b m_K^2 + c m_K^2 \log m_K^2$ [23], which fits the data well (see Fig. 5) and yields a finite non-zero value in the chiral limit.

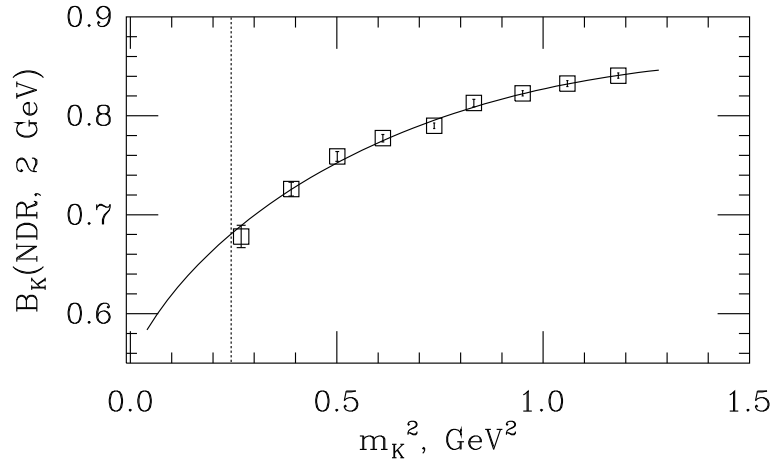


Figure 5: Parameter B_K in NDR $\overline{\text{MS}}$ scheme at 2 GeV on the dynamical ensemble vs. the meson mass squared. The fit is of the form $B_K = a + b m_K^2 + c m_K^2 \log m_K^2$. The vertical line here and in the other plots below marks the physical kaon mass.

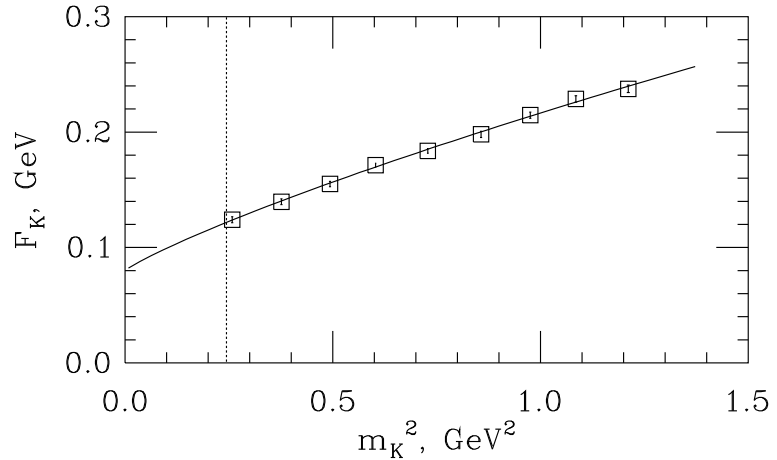


Figure 6: Pseudoscalar decay constant ($F = 93$ MeV in continuum) on the dynamical ensemble vs. meson mass squared. The fit is of the same form as B_K .

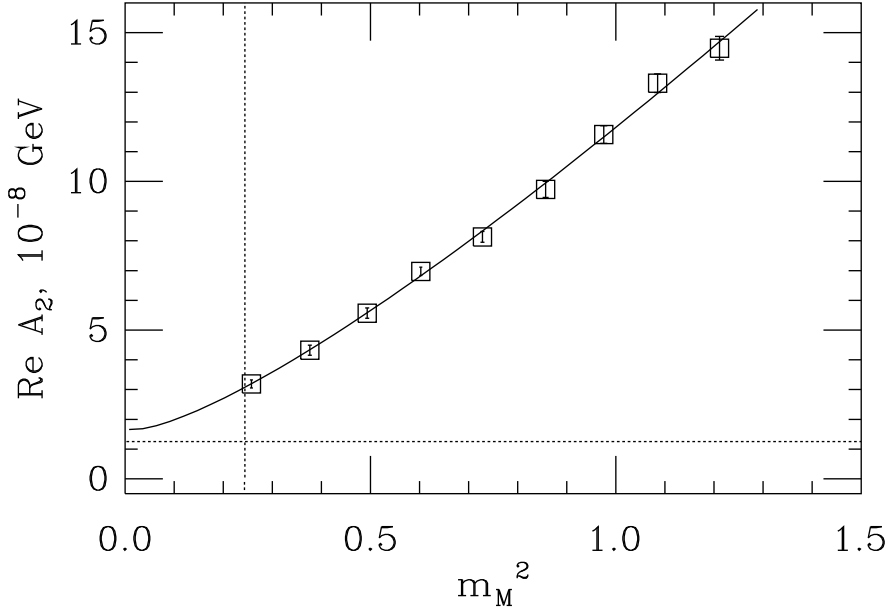


Figure 7: $Re A_2$ for the dynamical ensemble. The t is of the same form as B_K . The horizontal line is the experimental value of 1.25 GeV.

However, $Re A_2$ is proportional to the combination $B_K f$, and since both multipliers have a significant dependence on the meson mass (Figs. 5 and 6), the resulting $Re A_2$ is very sensitive to that mass. Fig. 7 shows the data for the dynamical ensemble, based on B_K values we have reported elsewhere [18]. Which meson mass should be used to read off the result becomes an open question. If known, the higher order chiral terms would remove this ambiguity. Forced to make a choice, we extrapolate to $M^2 = (m_K^2 + m^2)/2$.

Using our data [18] for B_K in quenched QCD and taking continuum limit we obtain¹ : $Re A_2 = 1.7 \cdot 10^8 \text{ GeV}$, to be compared with experimental $1.25 \cdot 10^8 \text{ GeV}$.

Higher order chiral corrections (including the meson mass dependence) are the largest systematic error in this determination. According to Golterman and Leung [16], one-loop corrections in (quenched) chiral perturbation theory can be as large as 60% or even 90%. Additional uncertainties (lattice spacing determination, quenching, finite volume, perturbative matching and statistical) are much smaller.

¹Note that the value obtainable from Fig. 7 is higher due to scaling violations. In our scheme $Re A_2$ is proportional to $B_K (f_K^{\text{latt}})^2 = 145 \text{ MeV}$. At $a \neq 0$ both B_K and f_K are higher than in the continuum limit.

4.2 ReA_0 results

We work in the normalization in which $\text{ReA}_0 = 27.8 \cdot 10^8 \text{ GeV}$, which is consistent with the normalization used for ReA_2 . Using Eqs. (22,23), ReA_0 can be expressed as

$$\text{ReA}_0 = \frac{G_F}{2} V_{ud} V_{us} \frac{m_K^2}{f} \sum_i z_i R_i;$$

where z_i are Wilson coefficients and

$$R_i = \frac{h^+ \mathcal{P}_i^{1=2} \mathcal{K}^+ i_s}{m^2} :$$

The subscript s indicates that these matrix elements already include subtraction of $h^+ \mathcal{P}_{\text{sub}} \mathcal{K}^+ i$. All contraction types, including the expensive "eye" and "annihilation", need to be calculated. $\mathcal{O}_i^{1=2}$ are isospin 1/2 parts of the operators \mathcal{O}_i . For example,

$$\mathcal{O}_1^{1=2} = \frac{2}{3} (\bar{s}d)_{LL} (\bar{u}u)_{LL} - \frac{1}{3} (\bar{s}u)_{LL} (\bar{u}d)_{LL} + \frac{1}{3} (\bar{s}d)_{LL} (\bar{d}d)_{LL} \quad (24)$$

$$\mathcal{O}_2^{1=2} = \frac{2}{3} (\bar{s}u)_{LL} (\bar{u}d)_{LL} - \frac{1}{3} (\bar{s}d)_{LL} (\bar{u}u)_{LL} + \frac{1}{3} (\bar{s}d)_{LL} (\bar{d}d)_{LL} : \quad (25)$$

The results for quenched $= 6.0$ and 6.2 ensembles are shown in Figs. 8. The dependence on the meson mass is small, so there is no big ambiguity about the mass prescription as in the ReA_2 case. Some lattice spacing dependence may be present (Fig. 9), although the statistics for $= 6.2$ ensemble is too low at this moment to say for sure.

The effect of the final state interactions (contained in the higher order terms of the chiral perturbation theory) is likely to be large (and positive). This is the biggest and most poorly estimated uncertainty.

A perturbative uncertainty arises due to mixing of \mathcal{O}_2 with \mathcal{O}_6 operator through penguin diagrams in lattice perturbation theory. This is explained in the Section 5.1. We estimate this uncertainty at 10% for all ensembles.

As for other uncertainties, we have checked the lattice volume dependence by comparing ensembles Q_1 and Q_2 (1.6 and 3.2 fm at $= 6.0$). The effect was found to be small, so we consider $(1.6 \text{ fm})^3$ as a volume large enough to hold the system. We have also checked the effect of quenching and found it to be small compared to noise.

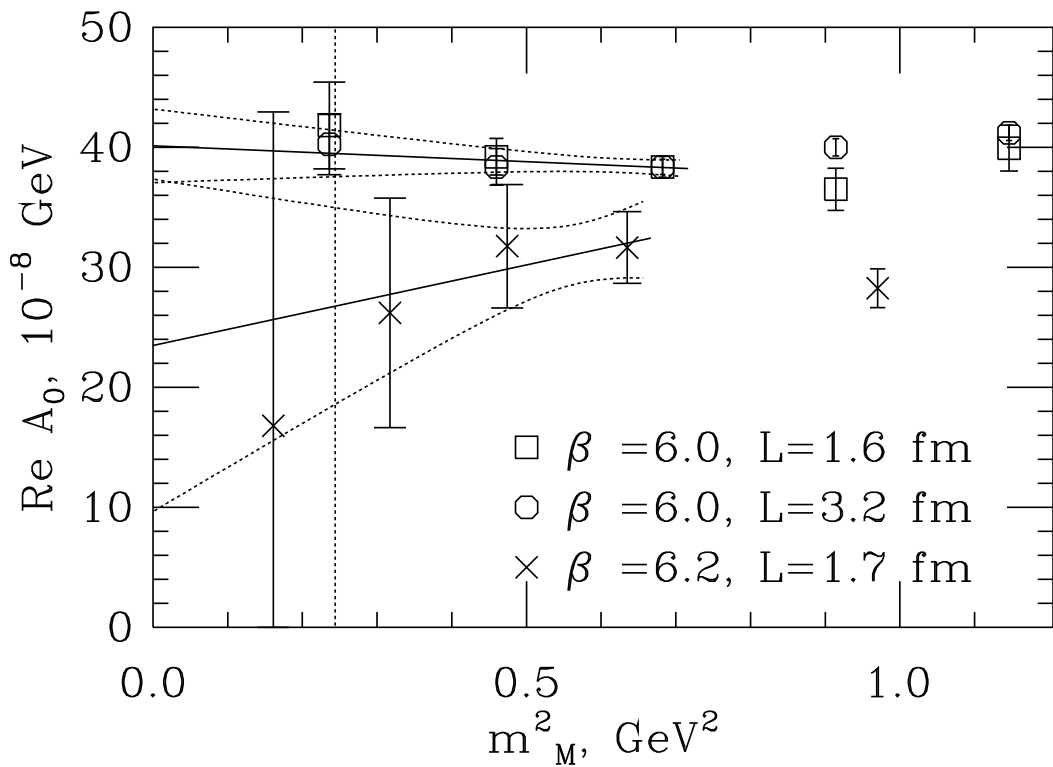


Figure 8: $\text{Re } A_0$ for quenched ensembles plotted against the meson mass squared. The upper group of points is for ensembles Q_1 and Q_2 , while the lower group is for Q_3 . Only statistical errors are shown.

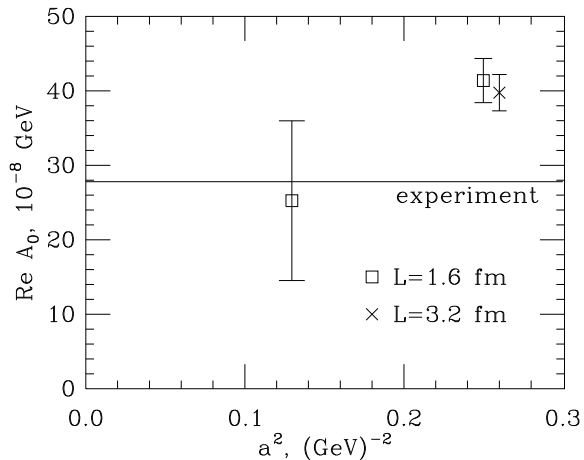


Figure 9: $\text{Re } A_0$ for quenched ensembles plotted against lattice spacing squared. The horizontal line shows the experimental result of $27.8 \times 10^8 \text{ GeV}$. Only statistical errors are shown.

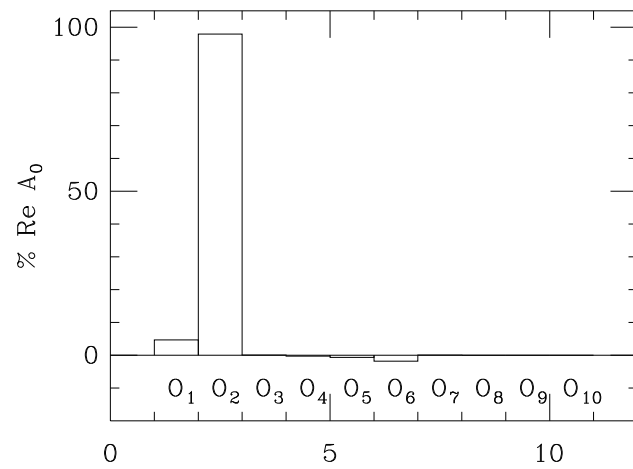


Figure 10: Contribution of various operators to $\text{Re } A_0$.

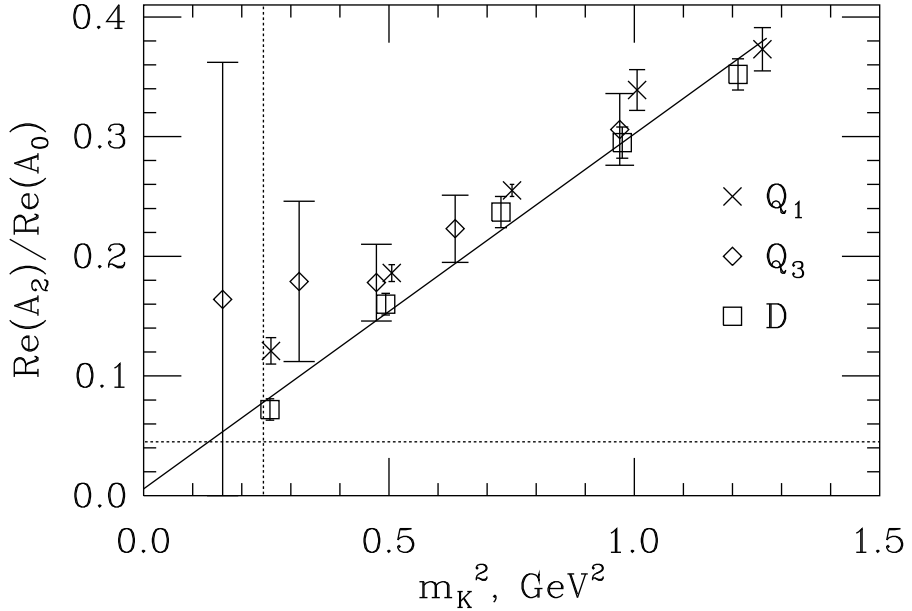


Figure 11: Ratio of $\text{Re}A_2/\text{Re}A_0$ versus the meson mass squared for quenched and dynamical ensembles. Ensembles Q_1 and D have comparable lattice spacings. The dynamical ensemble data were used for the fit. The big slope of the fit line is accounted for by the mass dependence of $\text{Re}A_2$. The horizontal line shows the experimental value of $1/22$. The error bars show only the statistical errors obtained by jackknife.

The breakdown of contributions of various basis operators to $\text{Re}A_0$ is shown in Fig. 10. By far, O_2 plays the most important role, while penguins have only a minor influence.

4.3 Amplitude ratio

Shown in Fig. 11 is the ratio $\text{Re}A_2/\text{Re}A_0$ as directly computed on the lattice for quenched and dynamical data sets. The data exhibit strong dependence on the meson mass, due to $\text{Re}A_2$ chiral behaviour (compare with Fig. 7). The result is roughly of the same order of magnitude as experiment. Clearly, higher order chiral terms are needed to say more on this subject. Other systematic errors are the same as those described in the previous Subsection.

5 Operator matching

As mentioned before, we have computed the matrix elements of all relevant operators. These are regulated in the lattice renormalization scheme. To get physical results, operators need to be matched to the same scheme in which the Wilson coefficients were computed, namely continuum \overline{MSNR} .

5.1 Perturbative matching and ReA_0

Matching of lattice and continuum operators can be done perturbatively:

$$O_i^{\text{cont}}(q) = O_i^{\text{lat}} + \frac{g^2(q a)^X}{16^2} \sum_j (C_{ij} \ln(\frac{q a}{\Lambda}) + C_{ij}) O_j^{\text{lat}} + O(g^4) + O(a^n); \quad (26)$$

where C_{ij} is the one-loop anomalous dimension matrix (the same in continuum and on the lattice), and C_{ij} are finite coefficients calculated in one-loop lattice perturbation theory [22, 21]. We use the "horizontal matching" procedure [17], whereby the same coupling constant as in continuum ($g_{\overline{MS}}$) is used. The operators are matched at an intermediate scale q and evolved using continuum renormalization group equations to the reference scale Λ , which we take to be 2 GeV.

In the calculation of ReA_0 and ReA_2 , the main contributions come from left-left operators. One-loop renormalization factors for such (gauge-invariant) operators were computed by Ishizuka and Shizawa [22] (for current-current diagrams) and by Patel and Sharpe [21] (for penguins). These factors are fairly small, so at a first glance the perturbation theory seems to work well, in contrast to the case of some operators essential for estimates of " $^{0=}$ ", as described below. However, even in the case of ReA_0 there is a certain ambiguity due to mixing of O_2 operator with O_6 through penguin diagrams. The matrix element of O_6 is rather large, so it heavily influences ReA_0 in spite of the small mixing coefficient. Operator O_6 receives huge renormalization corrections in the first order, as discussed below. The uncertainty in ReA_0 is associated with the higher-order diagrams for the mixing coefficient (Fig. 14b and 14d), which are likely to make a large contribution. We have resummed part of these diagrams (namely, all diagrams such as the one in Fig. 14b) by using a partially non-perturbative estimate of renormalization of operator PP_{EU} , as described below. The effect of ignoring the rest of the higher-order diagrams (such as Fig. 14d) is estimated by comparing with just one-loop renormalization. Thus an additional uncertainty of about 10% should be ascribed to the quoted values of ReA_0 .

In calculating of " $^{0=}$ " the operator matching issue becomes a much more serious obstacle as explained below.

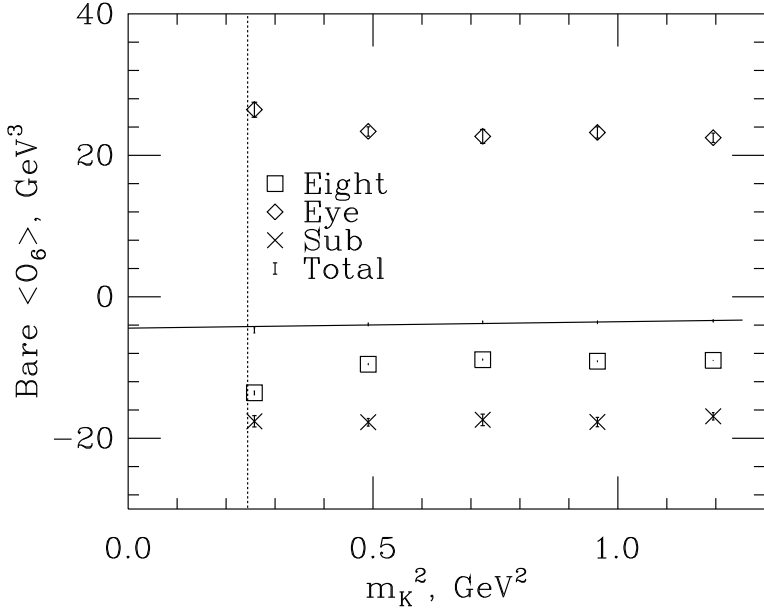


Figure 12: Three contributions to bare matrix element: \eight" (boxes), \eye" (diamonds) and \subtraction" (crosses). These data represent bare operators for the dynamical ensemble. The fit is done for the sum total of all contributions. All errors were combined by jackknife.

5.2 Problems with perturbative matching

The value of " \mathcal{Q} " depends on a number of subtle cancellations between matrix elements. In particular, O_6 and O_8 have been so far considered the most important operators whose contributions have opposite signs and almost cancel. The matrix element of each individual operator contains three main components ("eights", "eyes", and "subtractions"), which again conspire to almost cancel each other (see Fig. 12). Finally, contractions with left-right operators entering the expression for O_6 compete with $(P - S)(P + S)$ operators, because the latter receive large renormalization corrections and are made of comparable size with the former. Thus " \mathcal{Q} " is extremely sensitive to each of these components, and in particular to their matching.

Table 2: hO_6 in arbitrary units with one-loop perturbative matching using two values of q for Q_1 ensemble. For comparison, the results with no matching ("bare") are given.

Quark mass	0.01		0.02		0.03		0.04		0.05	
$q = 1-a$	0.1	1.2	0.9	0.4	1.2	0.2	1.6	0.3	1.1	0.2
$q = -a$	13.1	1.8	9.0	0.5	7.1	0.3	6.3	0.5	4.6	0.5
Bare	55.6	5.0	35.4	1.5	27.0	0.9	22.3	1.4	16.4	1.5

Consider contractions with operators such as²

$$(P P)_{EU} = (\bar{s}_5 \quad 5 u) \quad (\bar{u}_5 \quad 5 d) \quad (27)$$

$$(S S)_{IU} = (\bar{s} 1 \quad 1 d) \quad (\bar{d} 1 \quad 1 d) \quad (28)$$

$$(P S)_{AU} = (\bar{s}_5 \quad 5 d) \quad (\bar{d} 1 \quad 1 d); \quad (29)$$

which are main parts of, correspondingly, "eight", "eye" and "subtraction" components of O_6 and O_8 (see the Appendices). The finite coefficients for these operators have been computed at one-loop order in Ref. [21]. The diagonal coefficients are very large, so the corresponding one-loop corrections are in the neighborhood of 100%. In addition, they strongly depend on which q is used (refer to Table 2). Thus perturbation theory fails in reliably matching the operators in Eqs. (27{29).

The finite coefficients for other (subdominant) operators, such as $(P P)_{EF}$, $(S S)_{EU}$ and $(S S)_{EF}$, are not known for formulation with gauge-invariant operators³. For illustration purposes, in Table 2 we have used coefficients for gauge non-invariant operators computed in Ref. [21], but strictly speaking this is not justified.

To summarize, perturbative matching does not work and some of the coefficients are even poorly known. A solution would be to use a non-perturbative matching procedure, such as described by Donini et al. [24]. We have not completed this procedure. Nevertheless, can we say anything about " $^0=$ " at this moment?

² We apologize for slightly confusing notation: we use the same symbols here for operators and in the Appendices for types of contractions.

³ Patel and Sharpe [21] have computed corrections for gauge-noninvariant operators. Operators in Eqs. (27){(29) have zero distances, so the corrections are the same for gauge invariant and non-invariant operators. Renormalization of other operators (those having non-zero distances) differs from the gauge-noninvariant operators.

5.3 Partially nonperturbative matching

As a temporary solution, we have adopted a partially nonperturbative operator matching procedure, which makes use of bilinear renormalization coefficients Z_P and Z_S . We compute the latter [20] following the non-perturbative method suggested by Martinelli et al. [25]. Namely we study the inverse of the ensemble-averaged quark propagator at large off-shell momenta in a fixed (Landau) gauge. An estimate of the renormalization of four-fermion operators can be obtained as follows.

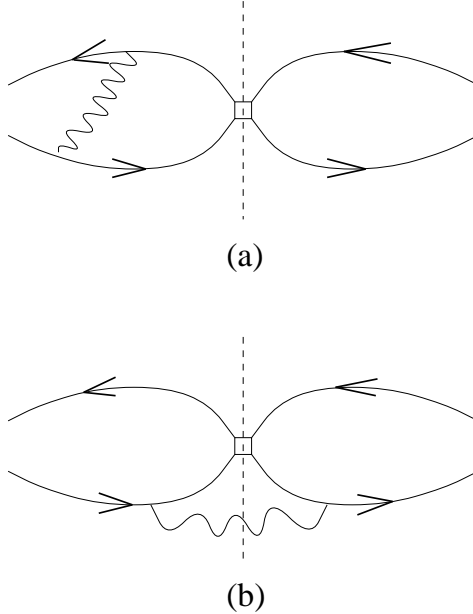


Figure 13: Example of two kinds of one loop diagrams possible in renormalization of four-fermion operators: (a) gluon crosses the axis, and (b) the rest of the diagrams.

Consider renormalization of the pseudoscalar{pseudoscalar operator in Eq. (27). At one-loop level, the diagonal renormalization coefficient C_{PP} (involving diagrams shown in Fig. 13) is almost equal to twice the pseudoscalar bilinear correction C_P . This suggests that, at least at one-loop level, the renormalization of $(PP)_{EU}$ comes mostly from diagrams in which no gluon propagator crosses the vertical axis of the diagram (for example, diagram (a) in Fig. 13), and very little from the rest of the diagrams (such as diagram (b) in Fig. 13). In other words, the renormalization of $(PP)_{EU}$ would be identical to the renormalization of

product of two pseudoscalar bilinears, were it not for the diagrams of type (b), which give a subdominant contribution. Mathematically,

$$(PP)_{EU}^{\text{cont}} = (PP)_{EU}^{\text{latt}} Z_{PP} + \dots;$$

where

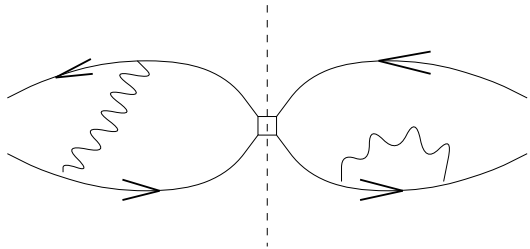
$$Z_{PP} = Z_P^2 (1 + \frac{g^2}{16^2} C_{PP} + O(g^4)); \quad (30)$$

$$Z_P = 1 + \frac{g^2}{16^2} C_P + O(g^4); \quad (31)$$

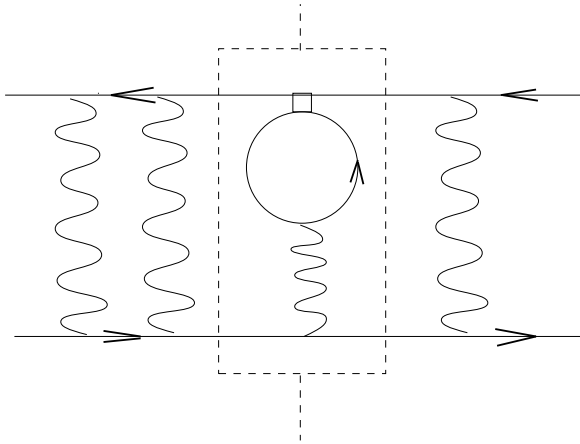
and dots indicate mixing with other operators (non-diagonal part). The factor $C_{PP} - 2C_P$ contains diagrams of type (b) and is quite small.

In order to proceed, it may be reasonable to assume that the same holds at all orders in perturbation theory, namely the diagrams of type b in Fig. 13 give subdominant contribution. This assumption should be verified separately by performing non-perturbative renormalization procedure for four-fermion operators. If this ansatz is true, we can substitute the non-perturbative value of Z_P into Eq. (30) instead of using the perturbative expression from Eq. (31). Thus a partially nonperturbative estimate of $(PP)_U^{\text{cont}}$ is obtained. This procedure is quite similar to the tadpole improvement idea: the bulk of diagonal renormalization is calculated non-perturbatively, while the rest is reliably computed in perturbation theory. Analogously we obtain diagonal renormalization of operators $(SS)_{IU}$ and $(PP)_{A2U}$ by using $Z_{SS} = Z_S^2 (1 + \frac{g^2}{16^2} C_{SS} + O(g^4))$ and $Z_{PS} = Z_S Z_P (1 + \frac{g^2}{16^2} C_{PS} + O(g^4))$. We note that $Z_P \neq Z_S$, even though they are equal in perturbation theory. We match operators at the scale $q = 1=a$ and use continuum two-loop anomalous dimension to evolve to $q=2$ GeV.

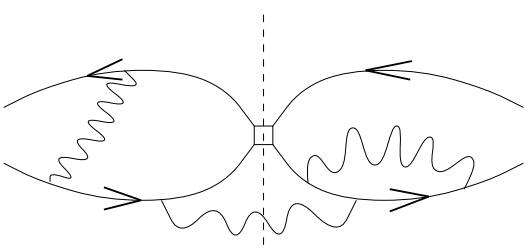
Unfortunately, the above procedure does not solve completely the problem of operator renormalization, since it deals only with diagonal renormalization of the zero-distance operators in Eqs. (27 | 29). Even though these operators are dominant in contributing to " --- ", other operators (such as $(SS)_{EU}$ and $(PP)_{EF}$) can be important due to mixing with the dominant ones. The mixing coefficients for these operators are not known even in perturbation theory. For a reasonable estimate, we vary them from zero to twice their value obtained for gauge non-invariant operator mixing [21]. The resulting variation in " --- " is reasonably small, even though the variations of subdominant operators' matrix elements are huge.



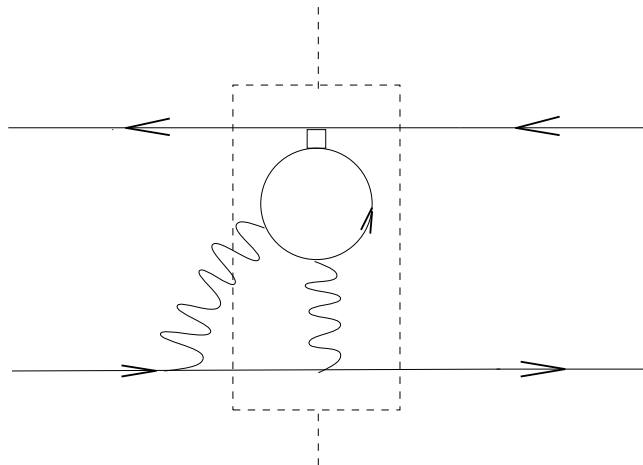
(a)



(b)



(c)



(d)

Figure 14: Example of four kinds of diagrams with arbitrary number of loops possible in renormalization of four-fermion operators: in (a) and (b) the gluon crosses neither the box nor the axis; (c) and (d) exemplify the rest of the diagrams. The rectangular drawn in dotted line corresponds to operator structure PP_{EU} .

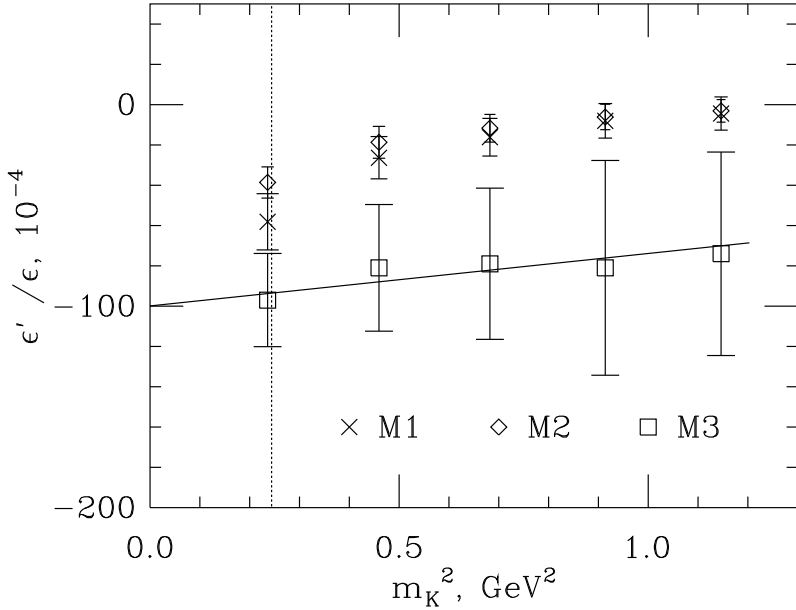


Figure 15: A rough estimate of " \mathbb{Q}_1 " for Q_1 ensemble using the partially nonperturbative procedure described in text. Three sets of points correspond to using experimental $\text{Re}A_0$ and $\text{Re}A_2$ in the Eq. (15) (crosses), using our $\text{Re}A_0$ but experimental (diamonds), or using $\text{Re}A_0$ and $\text{Re}A_2$ obtained from our calculations (squares). The latter method is preferred because arguably it amounts to cancelling uncertainties coming from the final state interactions (in other words, we obtain the final state interaction factors from comparing our computed $\text{Re}A_0$ and $\text{Re}A_2$ with experiment, and use them to compute the imaginary parts of these amplitudes). To obtain these numbers, we have used $\text{Im } t = 1.5 \cdot 10^4$. The error is a combination of statistical error (obtained by combining the errors in matrix elements by jackknife), a matching error coming from uncertainties in the determination of Z_P and Z_S , and an uncertainty in non-diagonal mixing of subdominant operators.

Secondly, since renormalization (either perturbative or non-perturbative) of operators $(PP)_{EU}$, $(SS)_{IU}$ and $(PS)_{A2U}$ is dramatic, their influence on other operators through non-diagonal matching is ambiguous at one loop order, even if the matching coefficients are known. The ambiguity is due to higher order diagrams (for example, those shown in Fig. 14). In order to partially resum them we use operators $(PP)_{EU}$, $(SS)_{IU}$ and $(PS)_{A2U}$ multiplied by factors Z_P^2 , Z_S^2 and $Z_P Z_S$, correspondingly, whenever they appear in non-diagonal matching with other operators. This is equivalent to evaluating the diagrams of type (a) and (b) in Fig. 14 at all orders, but ignoring the rest of the diagrams (such as diagrams (c) and (d) in Fig. 14) at all orders higher than rst . To estimate a possible error in this procedure we compare with a simpler one, whereby bare operators are used in non-diagonal corrections. (The latter procedure is equivalent to using strictly one-loop corrections.)⁴ The estimated error in " η " is quite substantial.

6 Estimates of " η "

Within the procedure outlined in the previous section (and provided our assumptions are valid) we have found that $\text{Re} \eta$ has a different sign from the expected one. Thus our data favor negative or very slightly positive value of " η " (Tables 3 and 4 and Fig. 15). Finite volume and quenching effects are small compared to noise.

The main uncertainty in " η " comes from operator matching, diagonal and non-diagonal. For diagonal matching the uncertainty comes from (1) errors in the determination of Z_P and Z_S non-perturbatively and from (2) unknown degree of validity of our ansatz in Sec. 5.3. For non-diagonal matching, the error is due to (1) unknown non-diagonal coefficients in matching matrix and (2) ambiguity of accounting higher-order corrections. In the Tables 3 and 4 these two classes of errors are represented separately, in addition to statistical error. The diagonal and non-diagonal matching errors are of comparable size.

The uncertainty due to operator matching is common to any method to compute the relevant matrix elements on the lattice (at least, with staggered fermions). In addition, our method has an inherent uncertainty due to dropping the higher order chiral terms. Lattice spacing dependence of " η " is unclear at this point, but it may be significant.

Thus " η " is an extremely fragile quantity. The rough estimates in Tables 3 and 4 should be used with extreme caution.

⁴ A completely analogous scheme was used for matching of O_6 with O_2 through penguins when evaluating $\text{Re} A_0$.

7 Conclusion

We have presented in detail the setup of our calculation of weak hadronic matrix elements relevant for $I = 1=2$ rule and " $0=$ ". We have obtained statistically significant data for all basis operators.

The simulation results for $I = 1=2$ rule are roughly consistent with the experimental data. However, the uncertainty due to higher order chiral terms is very large. If these terms are calculated in the future, a more definite prediction for physical amplitudes can be obtained using our present data for matrix elements (the latter are the bulk of our work). The matrix elements should be computed at a few more values of μ in the future in order to take continuum limit.

In addition to the issues mentioned above, the calculation of " $0=$ " is complicated by the failure of perturbation theory in operator matching. We give our crude estimates, but in order to achieve real progress the full nonperturbative matching procedure should be performed.

We appreciate L. Venkataraman's help in developing CRAY-T3E software. We thank the Ohio Supercomputing Center and National Energy Research Scientific Computing Center (NERSC) for the CRAY-T3E time. We thank Columbia University group for access to their dynamical configurations.

Appendix 1: Explicit expressions for fermion contractions

.1 Quark operators

We work in the two flavor traces formalism when calculating contractions with four-fermion operators: for each contraction separately the operators are rendered in the form (if necessary, by Fierz transformation) of two bilinears with the flavor in the form of a product of two flavor traces. To be more precise, for "eights" contractions the operators are rendered in the form $(\bar{s} u)(\bar{u} d)$, while for the "eye" and "annihilation" contractions the appropriate form is $(\bar{s} d)(\bar{q} q)$. This is done in continuum, before assigning the staggered fermion flavor.

The operator transcription in flavor space for staggered fermions is now standard [9], and we give it here for completeness. The Goldstone bosons have spin-flavor structure $5 \bar{5}$. The flavor structure of the operators is defined by requiring non-vanishing of the flavor traces, and so it depends on the contraction type: the flavor structure is 5 in "eights" and two-point functions, 1 in "eyes" and "subtractions". In "annihilation" contractions the flavor structure is 1 for the bilinear in the quark loop trace and 5 for the one involved in the

external trace.

Either one or two color traces may be appropriate for a particular contraction with a given operator (see the next Appendix section for details). In one trace contractions (type "\F" for "Ferzed") the color flow is exchanged between the bilinears, while in two trace contractions (type "\U" for "Unferzed") the color flow is contained within each bilinear so that the contraction is the product of two color traces. In either contraction type, when the distance between staggered fermion fields being color-connected is non-zero, a gauge connector is inserted in the gauge-invariant fashion. The connector is computed as the average of products of gauge links along all shortest paths connecting the two sites. We also implement tadpole improvement by dividing each link in every gauge connector by $u_0 = (1=3\text{Tr}(U_P))^{1/4}$, where U_P is the average plaquette value.

2 Sources and contractions

We use local U(1) pseudofermion wall sources. Explicitly, we set up a field of U(1) phases $(x; t_0)$ ($j = 1$) for each color and each site at a given time slice t_0 , which are chosen at random and satisfy

$$h(x; t_0) \cdot (y; t_0) = 1; \quad x, y$$
 (32)

(Boldface characters designate spatial parts of the 4-vector with the same name.) We proceed to explain how this setup works in the case of the two-point function calculation, with trivial generalization to "flight" and "annihilation" contractions.

Consider the propagator from a wall at $t_0 = 0$ in a given background gauge configuration, computed by inverting the equation

$$(\mathcal{D} + m)_{x,y} (y) = \langle x; 0 \rangle_{x,y,0} \quad (33)$$

This is equivalent to computing

$$\langle y \rangle = \sum_x \langle x; 0 \rangle G(x; y; 0); \quad (34)$$

where $G(y; x)$ is the propagator from 4-point x to 4-point y . For staggered fermions description we label the fields by hypercube index h and the hypercube corner indices $A \in \{0, 1\}^4$ instead of y . The two-point function is constructed as follows:

$$\text{TP} / \sum_{h,A}^X \langle h; A \rangle U(h; A; A +) \langle h; A + \rangle \langle A \rangle (-1)^A; \quad (35)$$

where $\langle A \rangle$ and $\langle \cdot \rangle$ are phases and distances appropriate for a given staggered fermion operator, $U(h; A; A +)$ is the appropriate gauge connector (see below), modulo 2 summation is

implied for hypercube indices A , and h runs over all hypercubes in a given time slice where the operator is inserted. The factor $(-1)^A$ takes into account that for staggered fermions $G(x; y) = G^y(y; x) (-1)^x (-1)^y$. Equation (35) corresponds to

$$TP / \sum_{x,y,z}^X G(x; y) G(y; z) (-1)^z (z) (x); \quad (36)$$

where \sum is used for simplicity to show the appropriate operator structure. The summation over x and z over the entire spatial volume averages over noise, so the last equation is equivalent to

$$TP / \sum_{x,y}^X \text{tr} G(x; y) G(y; x) (-1)^x; \quad (37)$$

Therefore, using the pseudofermion wall source is equivalent to summation of contractions obtained with independent local delta-function sources. Note that the factor $(-1)^x$ and zero distance in the staggered fermion language are equivalent to spin-flavor structure $5 \bar{5} \bar{5} \bar{5}$. This means the source creates pseudoscalar mesons at rest, which includes Goldstone bosons. Strictly speaking, this source also creates mesons with spin-flavor structure $5 \bar{4} \bar{5} \bar{4}$, since it is defined only on one time slice. However, as explained in the first footnote in Section 2.3 of Ref. [9], these states do not contribute.

We have used one copy of pseudofermion sources per configurations.

Analogously, we construct the pion sink at time T by using another set of $U(1)$ random noise $(h^y(x; T) - y; T))_{i=1, x, y, j=1}$. The propagator is computed as follows:

$$(D + m)_{x,y} (y) = (x; T)_{x,y,T}; \quad (38)$$

Suppose $1, 2 \in f0;1g^4$ and $1(A), 2(A)$ are distances and phases of the two staggered fermion bilinears making up a given four-fermion operator. The expression for the "eight" contraction (Fig. 1a) with two color traces ("U" type) is given by

$$E_U / \sum_{h;A,B}^X (h; A) U (h; A; A + 1) (h; A + 1) 1(A) (-1)^A (h; B) U (h; B; B + 2) (h; B + 2) 2(B) (-1)^B; \quad (39)$$

up to various normalization factors which cancel in the B ratio. In this expression $A, B \in f0;1g^4$ run over 16 hypercube corners (modulo 2 summation is implied for these indices). The hypercube index h , as before, runs over the entire spatial volume of the time t of the operator insertion. The gauge connector $U(h; A; B)$ is the identity matrix when $A = B$, otherwise it is the average of products of gauge links in the given configuration along all shortest paths from A to B in a given hypercube h . The expression 39, as well as all the

other contractions, is computed for each background gauge configurations and subject to averaging over the configurations. (Whenever several of contractions are combined in a single quantity, such as a B ratio, we use jackknife to estimate the errors).

The expression for one color trace ("F" type) contraction is similar:

$$E_F / \sum_{h;A,B}^X (h;A)U (h;A;B + \dots) (h;A + \dots) (A) (-1)^A (h;B)U (h;B;A + \dots) (h;B + \dots) (B) (-1)^B; \quad (40)$$

For "\eye" and "\subtraction" diagrams (Fig. 11 and 1d) the source setup is a little more involved, since the kaon and pion are directly connected by a propagator. In order to construct a wall source we need to compute the product

$$(y) = \sum_x^X G(y; t; x; T) G(x; T; 0; 0) (-1)^x;$$

In order to avoid computing propagators from every point x at the timeslice T , we first compute propagator $G(x; T; 0; 0)$, cut out the timeslice T and use it as the source for calculating the propagator to $(y; t)$. This amounts to inverting equation

$$(D + m)_{x,y} (y) = (x)_{(x_4; T)} (-1)^x; \quad (41)$$

where (x) is the propagator from the wall source at $t_0 = 0$ defined in Eq. (33). We use the following expression for evaluating the "\subtraction" diagram:

$$S / \sum_{h;A}^X (h;A)U (h;A;A + \dots) (h;A + \dots) (A) (-1)^A; \quad (42)$$

Again, averaging over the noise leaves only local connections in both sources, so in the continuum language we get:

$$S / \sum_{x,y,z}^X \text{tr} G(x; 0; z; t) G(z; t; y; T) G(y; T; x; 0) (-1)^x (-1)^y; \quad (43)$$

In order to efficiently compute fermion loops for "\eye" and "\annihilation" diagrams (Fig. 1b and 1c), we use $U(1)$ noise copies $^{(i)}$, $i = 1, \dots, N$, at every point in space-time. We compute $^{(i)}$ by inverting $(D + m)_{x,y}^{(i)} = \delta_{x,y}^{(i)}$. It is easy to convince oneself that the propagator from y to x equals

$$G(x; y) = h_{x,y}^{(i)}; \quad (44)$$

In practice we average over $N = 10$ noise copies. This includes 2 or 4 copies of the lattice in time extension, so the real number of noise copies is 20 or 40, with another factor of 3 for color. The efficiency of this method is crucial for obtaining good statistical precision.

The expression for "U" and "F" type "eye" diagram s are as follows:

$$\mathbb{I}_U / \sum_{h;A;B}^X (h;A)U (h;A;A + \gamma_1) (h;A + \gamma_1) \gamma_1 (A) (-1)^A$$

$$\frac{1}{N} \sum_{i=1}^N \sum_{h;B}^X (h;B)U (h;B;B + \gamma_2) \stackrel{(i)}{(h;B + \gamma_2) \gamma_2 (B)} (-1)^B; \quad (45)$$

$$\mathbb{I}_F / \sum_{h;A;B}^X (h;A)U (h;A;B + \gamma_2) (h;A + \gamma_1) \gamma_1 (A) (-1)^A$$

$$\frac{1}{N} \sum_{i=1}^N \sum_{h;B}^X (h;B)U (h;B;A + \gamma_1) \stackrel{(i)}{(h;B + \gamma_1) \gamma_1 (B)} (-1)^B; \quad (46)$$

The computation of "annihilation" diagrams (Fig. 1c) is similar to the two-point function, except the fermion loop is added and the derivative with respect to quark mass difference $m_d - m_s$ is inserted in turn in every strange quark propagator. Derivatives of the propagators are given by inverting equations

$$(\not{D} + m)^0 = ; \quad (47)$$

$$(\not{D} + m)^0 \stackrel{(i)}{=} : \quad (48)$$

We have then four kinds of "annihilation" contractions, which should be combined in an appropriate way for each operator depending on the quark flavor structure (this is spelled out in the next Appendix section):

$$A_{1U} / \sum_{h;A;B}^X \stackrel{0}{(h;A)U} (h;A;A + \gamma_1) (h;A + \gamma_1) \gamma_1 (A) (-1)^A$$

$$\frac{1}{N} \sum_{i=1}^N \sum_{h;B}^X \stackrel{(i)}{(h;B)U} (h;B;B + \gamma_2) \stackrel{(i)}{(h;B + \gamma_2) \gamma_2 (B)} (-1)^B; \quad (49)$$

$$A_{1F} / \sum_{h;A;B}^X \stackrel{0}{(h;A)U} (h;A;B + \gamma_2) (h;A + \gamma_1) \gamma_1 (A) (-1)^A$$

$$\frac{1}{N} \sum_{i=1}^N \sum_{h;B}^X \stackrel{(i)}{(h;B)U} (h;B;A + \gamma_1) \stackrel{(i)}{(h;B + \gamma_1) \gamma_1 (B)} (-1)^B; \quad (50)$$

$$A_{2F} / \frac{1}{N} \sum_{i=1}^N \begin{array}{c} X \\ \hbar; A, B \end{array} \stackrel{(i)}{=} (h; B) U (h; B; B + \dots)_2 \stackrel{0(i)}{=} (h; B + \dots)_2 (B) (-1)^B; \quad (51)$$

$$\frac{1}{N} \sum_{i=1}^N \begin{array}{c} X \\ \hbar; A, B \end{array} \stackrel{(i)}{=} (h; A) U (h; A; B + \dots)_2 \stackrel{0(i)}{=} (h; A + \dots)_1 (A) (-1)^A; \quad (52)$$

(53)

Appendix 2: Explicit expressions for matrix elements in terms of fermion contractions.

First we give expressions for $I = 1=2$ parts of basis operators.

$$O_1^{1=2} = \frac{2}{3} (\bar{s} (1 \dots 5) d) (\bar{u} (1 \dots 5) u) - \frac{1}{3} (\bar{s} (1 \dots 5) u) (\bar{u} (1 \dots 5) d) \\ + \frac{1}{3} (\bar{s} (1 \dots 5) d) (\bar{d} (1 \dots 5) d) \quad (54)$$

$$O_2^{1=2} = \frac{2}{3} (\bar{s} (1 \dots 5) u) (\bar{u} (1 \dots 5) d) - \frac{1}{3} (\bar{s} (1 \dots 5) d) (\bar{u} (1 \dots 5) u) \\ + \frac{1}{3} (\bar{s} (1 \dots 5) d) (\bar{d} (1 \dots 5) d) \quad (55)$$

$$O_3^{1=2} = (\bar{s} (1 \dots 5) d) \stackrel{X}{\bar{q}} (1 \dots 5) q \quad (56)$$

$$O_4^{1=2} = (\bar{s} (1 \dots 5) d) \stackrel{q=u \neq d; s}{\bar{q}} (1 \dots 5) q \quad (57)$$

$$O_5^{1=2} = (\bar{s} (1 \dots 5) d) \stackrel{X}{\bar{q}} (1 + \dots 5) q \quad (58)$$

$$O_6^{1=2} = (\bar{s} (1 \dots 5) d) \stackrel{q=u \neq d; s}{\bar{q}} (1 + \dots 5) q \quad (59)$$

$$O_7^{1=2} = \frac{1}{2} [(\bar{s} (1 \dots 5) d) (\bar{u} (1 + \dots 5) u) - (\bar{s} (1 \dots 5) u) (\bar{u} (1 + \dots 5) d) \\ - (\bar{s} (1 \dots 5) d) (\bar{s} (1 + \dots 5) s)] \quad (60)$$

$$O_8^{1=2} = \frac{1}{2} [(\bar{s} (1 \dots 5) d) (\bar{u} (1 + \dots 5) u) - (\bar{s} (1 \dots 5) u) (\bar{u} (1 + \dots 5) d) \\ - (\bar{s} (1 \dots 5) d) (\bar{s} (1 + \dots 5) s)] \quad (61)$$

$$O_9^{1=2} = \frac{1}{2} [(\bar{s} (1 \quad 5) d) (\bar{u} (1 \quad 5) u) - (\bar{s} (1 \quad 5) u) (\bar{u} (1 \quad 5) d) - (\bar{s} (1 \quad 5) d) (\bar{s} (1 \quad 5) s)] \quad (62)$$

$$O_{10}^{1=2} = \frac{1}{2} [(\bar{s} (1 \quad 5) u) (\bar{u} (1 \quad 5) d) - (\bar{s} (1 \quad 5) d) (\bar{u} (1 \quad 5) u) - (\bar{s} (1 \quad 5) d) (\bar{s} (1 \quad 5) s)] \quad (63)$$

Expressions for and $I = 3=2$ parts of the operators are as follows:

$$O_1^{3=2} = O_2^{3=2} = \frac{2}{3} O_9^{3=2} = \frac{2}{3} O_{10}^{3=2} = \frac{1}{3} [(\bar{s} (1 \quad 5) u) (\bar{u} (1 \quad 5) d) + (\bar{s} (1 \quad 5) d) (\bar{u} (1 \quad 5) u) - (\bar{s} (1 \quad 5) d) (\bar{d} (1 \quad 5) d)] \quad (64)$$

$$O_7^{3=2} = \frac{1}{2} [(\bar{s} (1 \quad 5) u) (\bar{u} (1 + 5) d) + (\bar{s} (1 \quad 5) d) (\bar{u} (1 + 5) u) - (\bar{s} (1 \quad 5) d) (\bar{d} (1 + 5) d)] \quad (65)$$

$$O_8^{3=2} = \frac{1}{2} [(\bar{s} (1 \quad 5) u) (\bar{u} (1 + 5) d) + (\bar{s} (1 \quad 5) d) (\bar{u} (1 + 5) u) - (\bar{s} (1 \quad 5) d) (\bar{d} (1 + 5) d)] \quad (66)$$

$$O_3^{3=2} = O_4^{3=2} = O_5^{3=2} = O_6^{3=2} = 0 \quad (67)$$

(Whenever the color indices are not shown, they are contracted within each bilinear, i.e. there are two color traces.)

Let us introduce some notation. Each matrix element has three components:

$$h^+ \bar{p}_i \bar{K}^0 i = (E_i + I_i - S(2m_i)) \frac{m_K^2 - m^2}{(p - p_f)^2}; \quad (68)$$

where m is the common quark mass for s , d and u , and

$$_i = \frac{A_i}{TP}; \quad (69)$$

Here E_i and I_i stand for "eight" and "eye" contractions of the $\bar{p}_i \bar{K}^0 i$ matrix elements, $A_i = h^+ \bar{p}_i \bar{K}^0 i = (m_d - m_s)$ is the "annihilation" diagram for the given operator (or more precisely, its derivative with respect to mass difference $(m_d - m_s)$), $S = h^+ \bar{s} d \bar{K}^0 i$ is the "subtraction" diagram and $TP = h^+ \bar{s} d \bar{K}^0 i$ is the two-point function. We compute $_i$ by averaging the ratio in the right-hand side of Eq. (69) over a suitable time range.

Detailed expressions for E_i , I_i and A_i for each basis operator are given below in terms of basic contractions on the lattice. We label basic contractions by two letters, each representing a bilinear. For example, PP stands for contraction of the operator with spin structure $(\bar{5})(5)$, SS is for $(1)(1)$, VV stands for $(\bar{1})(1)$, and AA is for $(\bar{5})(\bar{5})$. The staggered flavor is determined by the type of contraction, as explained in the previous Appendix section. Basic contractions are also labeled by their subscript. The first letter indicates whether it is an "eight", "eye" or "annihilation" contraction, and the second is "U" for two, or "F" for one color trace. For example: PP_{EU} stands for "eight" type contraction of the operator with spin-flavor structure $(\bar{5})(5)(\bar{5})(5)$ with two color traces; VA_{A1F} stands for the annihilation contraction of the first type, in which the derivative is taken with respect to quark mass on the external leg (see the previous Appendix section), the spin-flavor structure is $(\bar{5})(\bar{5})(\bar{5})(1)$, and one color trace is used. What follows are the full expressions⁵.

"Eight" parts:

$$E_1^{1=2} = \frac{2}{3} (VV_{EF} + AA_{EF}) - \frac{1}{3} (VV_{EU} + AA_{EU}) \quad (70)$$

$$E_2^{1=2} = \frac{2}{3} (VV_{EU} + AA_{EU}) - \frac{1}{3} (VV_{EF} + AA_{EF}) \quad (71)$$

$$E_3^{1=2} = VV_{EF} + AA_{EF} \quad (72)$$

$$E_4^{1=2} = VV_{EU} + AA_{EU} \quad (73)$$

$$E_5^{1=2} = 2(PP_{EF} - SS_{EF}) \quad (74)$$

$$E_6^{1=2} = 2(PP_{EU} - SS_{EU}) \quad (75)$$

$$E_7^{1=2} = SS_{EF} - PP_{EF} + \frac{1}{2} (VV_{EU} - AA_{EU}) \quad (76)$$

$$E_8^{1=2} = SS_{EU} - PP_{EU} + \frac{1}{2} (VV_{EF} - AA_{EF}) \quad (77)$$

$$E_9^{1=2} = E_{10}^{1=2} = \frac{1}{2} (VV_{EF} + AA_{EF} - VV_{EU} - AA_{EU}) \quad (78)$$

$$E_1^{3=2} = E_2^{3=2} = \frac{2}{3} E_9^{3=2} = \frac{2}{3} E_{10}^{3=2} = \frac{1}{3} (VV_{EU} + AA_{EU} + VV_{EF} + AA_{EF}) \quad (79)$$

$$E_3^{3=2} = E_4^{3=2} = E_5^{3=2} = E_6^{3=2} = 0 \quad (80)$$

$$E_7^{3=2} = \frac{1}{2} (AA_{EU} - VV_{EU}) + SS_{EF} - PP_{EF} \quad (81)$$

⁵Signs of operators O_7 and O_8 have been changed in order to be consistent with the sign convention of Buras et al. [11].

$$E_8^{3=2} = \frac{1}{2} (AA_{EF} - VV_{EF}) + SS_{EU} - PP_{EU} \quad (82)$$

\Eye" parts:

$$I_1^{1=2} = VV_{IU} + AA_{IU} \quad (83)$$

$$I_2^{1=2} = VV_{IF} + AA_{IF} \quad (84)$$

$$I_3^{1=2} = 3(VV_{IU} + AA_{IU}) + 2(VV_{IF} + AA_{IF}) \quad (85)$$

$$I_4^{1=2} = 3(VV_{IF} + AA_{IF}) + 2(VV_{IU} + AA_{IU}) \quad (86)$$

$$I_5^{1=2} = 3(VV_{IU} - AA_{IU}) + 4(PP_{IF} - SS_{IF}) \quad (87)$$

$$I_6^{1=2} = 3(VV_{IF} - AA_{IF}) + 4(PP_{IU} - SS_{IU}) \quad (88)$$

$$I_7^{1=2} = 2(PP_{IF} - SS_{IF}) \quad (89)$$

$$I_8^{1=2} = 2(PP_{IU} - SS_{IU}) \quad (90)$$

$$I_9^{1=2} = VV_{IF} + AA_{IF} \quad (91)$$

$$I_{10}^{1=2} = VV_{IU} + AA_{IU} \quad (92)$$

\Annihilation" parts:

$$A_1^{1=2} = (VA_{A1U} + AV_{A1U}) \quad (93)$$

$$A_2^{1=2} = (VA_{A1F} + AV_{A1F}) \quad (94)$$

$$A_3^{1=2} = 3(VA_{A1U} + AV_{A1U}) (VA_{A2U} + AV_{A2U}) \\ 2(VA_{A1F} + AV_{A1F}) (VA_{A2F} + AV_{A2F}) \quad (95)$$

$$A_4^{1=2} = 3(VA_{A1F} + AV_{A1F}) (VA_{A2F} + AV_{A2F}) \\ 2(VA_{A1U} + AV_{A1U}) (VA_{A2U} + AV_{A2U}) \quad (96)$$

$$A_5^{1=2} = 3(VA_{A1U} - AV_{A1U}) (VA_{A2U} - AV_{A2U}) + 2(PS_{A2F} - SP_{A2F}) \quad (97)$$

$$A_6^{1=2} = 3(VA_{A1F} - AV_{A1F}) (VA_{A2F} - AV_{A2F}) + 2(PS_{A2U} - SP_{A2U}) \quad (98)$$

$$A_7^{1=2} = \frac{1}{2} (VA_{A2U} - AV_{A2U}) + (PS_{A2F} - SP_{A2F}) \quad (99)$$

$$A_8^{1=2} = \frac{1}{2} (VA_{A2F} - AV_{A2F}) + (PS_{A2U} - SP_{A2U}) \quad (100)$$

$$A_9^{1=2} = VA_{A1F} + AV_{A1F} + \frac{1}{2} (VA_{A2U} + AV_{A2U} + VA_{A2F} + AV_{A2F}) \quad (101)$$

$$A_{10}^{1=2} = VA_{A1U} + AV_{A1U} + \frac{1}{2} (VA_{A2F} + AV_{A2F} + VA_{A2U} + AV_{A2U}) \quad (102)$$

$$(103)$$

Of course, "eye" and "annihilation" contractions are not present in $I = 3=2$ operators.

References

- [1] G .D .Bar et al. (NA 31 CERN), Phys. Lett. B 317 (1993) 233.
- [2] G ibbons et al. (E 731 Ferm ilab), Phys. Rev. Lett 70 1203-1206, 1993.
- [3] G .K ilcup, Nucl. Phys. B (Proc. Suppl.) 20 (1991) 417 (LATTICE '90); S. Sharpe, R .G upta, G .G uralnik, G .K ilcup, A .P atel, Phys. Lett. 192B (1987) 149.
- [4] C .B emard, T .D raper, G .H ockney, A .S oni, Nucl. Phys. B (Proc. Suppl.) 4 (1988) 483 (LATTICE '87); C .B emard, A .E HK hadra, A .S oni, Nucl. Phys. Proc. Suppl. 7A (1989) 277;
- [5] C .B emard, A .S oni, Ferm ilab Lattice (1988) 0155; Nucl. Phys. B (Proc. Suppl.) 17 (1990) 495 (LATTICE '89).
- [6] M .B .G avela, L .M aiani, S .P etrarca, G .M artinelli, O .P ene, C .T .S adra jda, Nucl. Phys. (Proc. Suppl. 7A) (1989) 228; E .Franco, L .M aiani, G .M artinelli, A .M orelli, Nucl. Phys. B 317 (1989) 63; M .B .G avela, L .M aiani, S .P etrarca, G .M artinelli, O .P ene, Phys. Lett. 211 B (1988) 139; Nucl. Phys. B (Proc. Suppl.) 4 (1988) 466.
- [7] S .A okiet al. (JLQCD collaboration), Phys. Rev. D 58 (1998) 054503, hep-lat/9711046.
- [8] G .K ilcup, S .Sharpe, Nucl. Phys. B 283 (1987) 493.
- [9] S .Sharpe, A .P atel, R .G upta, G .G uralnik and G .K ilcup, Nucl. Phys. B 286 (1987) 253-292.
- [10] C .B emard, T .D raper, A .S oni, H .D .P olitzer and M .B .W ise, Phys. Rev. D 32 (1985) 2343.
- [11] A .B uras et al., Nucl. Phys. B 408 (1993) 209-285, hep-ph/9303284.
- [12] A .B uras et al., Nucl. Phys. B 400 (1993) 37 (hep-ph/9211304); Buras et al., Nucl. Phys. B 400 (1993) 75 (hep-ph/9211321).
- [13] L .M aiani, M .T esta, Phys. Lett. B 245 (1990) 585.

- [14] D .Chen, R M awhinney, Nucl.Phys.B (Proc. Suppl.) 53 (1997) 216 (LATTICE '96).
- [15] S.G ottlieb, Nucl.Phys.B (Proc Suppl.) 53 (1997) 155 (LATTICE '96).
- [16] M .G oltem an, K C .Leung, Phys. Rev.D 56 (1997) 2950, hep-lat/9702015.
- [17] R .G upta, T .Bhattacharya, S .Sharpe, Phys. Rev.D 55 (1997) 4036.
- [18] G .K ilcup, D .P ekurovsky, Nucl.Phys.B (Proc. Suppl.) 53 (1997) 345 (LATTICE '96), hep-lat/9609006.
- [19] JLQCD , Phys. Rev. Lett. 80 (1998) 5271.
- [20] D P ekurovsky, G .K ilcup, in preparation.
- [21] S .Sharpe, A .P atel, hep-lat/9310004.
- [22] N .I shizuka, Y .Shizawa, Phys. Rev.D 49 (1994) 3519, hep-lat/9308008.
- [23] S .Sharpe, Phys. Rev.D 46 (1992) 3146.
- [24] A .D onini, V .G inenez, G .M artinelli, G .C .R ossi, M .T alevi, M .T esta, A .V ladikas, Nucl.Phys.B (Proc. Suppl.) 53 (1997) 883 (LATTICE '96), hep-lat/9608108; A .D onini, G .M artinelli, C .T .S achrajda, M .T alevi, A .V ladikas, Phys. Lett. B 360 (1995) 83, hep-lat/9508020.
- [25] G .M artinelli, C .P ittori, C .T .S achrajda, M .T esta, A .V ladikas, Nucl.Phys.B 445 (1995) 81, hep-lat/9411010.

TABLES

Table 3: " η^0 " in units of 10^{-4} for Q_1 ensemble, computed in three ways: (M 1) $\text{Re}A_0$ and $\text{Re}A_2$ amplitudes values entering the expression for " η^0 " are taken from experiment; (M 2) η^0 amplitude ratio is taken from experiment, while $\text{Re}A_0$ amplitude is from our simulation; (M 3) both $\text{Re}A_0$ and $\text{Re}A_2$ are from our simulation. The third method is preferred because arguably it accounts to cancelling uncertainties coming from the final state interactions (in other words, we obtain the final state interaction factors by comparing our computed real parts of A_0 and A_2 with experiment, and use these factors in computation of the imaginary parts of the amplitudes). In all cases, partially nonperturbative matching have been used to obtain the results. The first error is statistical (obtained by combining the individual errors in matrix elements by jackknife). The second one is the estimated error in diagonal operator matching due to uncertainty in the determination of Z_P and Z_S . The third error is the estimated error in the non-diagonal part of operator matching. Some other parameters used in obtaining this result are: $\text{Im } t = 1.5 \cdot 10^4$, $m_t = 170 \text{ GeV}$, $m_b = 4.5 \text{ GeV}$, $m_c = 1.3 \text{ GeV}$, $\alpha_s = 0.25$, $\frac{\alpha_s}{\text{MS}}(2 \text{ GeV}) = 0.195$ (the latter is based on setting the lattice scale by meson mass). Short distance coefficients were obtained by two-loop running using the anomalous dimension and threshold matrices computed by Buras et al. [12]. Finite volume and quenching effects were found to be small compared to noise.

Quark mass	0.01				0.02				0.03			
M 1	58.1	2.1	10.6	8.8	26.3	0.8	8.9	5.5	16.1	0.4	8.0	4.8
M 2	38.6	2.1	6.0	4.4	18.7	0.3	7.0	3.7	11.7	0.2	6.0	3.4
M 3	97	14	13	13	81	4	23	21	79	2	27	26
Quark mass	0.04				0.05							
M 1	8.0	0.9	7.2	4.7	4.4	0.9	7.2	3.9				
M 2	6.1	0.5	5.3	3.5	3.1	0.5	4.9	2.7				
M 3	81	5	38	37	74	4	38	33				

Table 4: "0=" results for Q_3 ensemble ($\beta = 6.2$). Everything else is the same as in Table 3.

Quark mass	0.010				0.015			
M 1	109	15	84	21	64	7	63	25
M 2	39	9	22	5	22	2	18	4
M 3	30.0	4.1	23.2	5.8	21.1	2.3	20.7	8.2
Quark mass	0.020				0.030			
M 1	36	4	60	11	19	2	38	6
M 2	13.7	0.6	20	4	9.5	0.6	17	3
M 3	15.9	1.8	26.5	4.9	10.8	1.1	21.6	3.4